Open Access

Beam Shaping Freeform Lens Design With Modified Optical Flux Partition

Pin Han
Hsun-Ching Hsu
Cheng-Mu Tsai
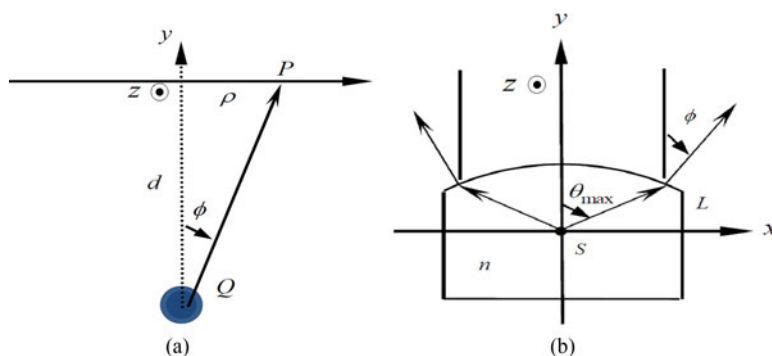
IEEE

Beam Shaping Freeform Lens Design With Modified Optical Flux Partition

Pin Han ⓘ **, Hsun-Ching Hsu** ⓘ **, and Cheng-Mu Tsai** ⓘ

Graduate Institute of Precision Engineering, National Chung Hsing University,
Taichung 402, Taiwan

Abstract: A freeform lens design strategy that performs directivity transformation is proposed. In principle, arbitrary beam pattern can be achieved with this method, which uses a modified flux partition method. Taking a Lambertian light source as the example, this method successfully give different required intensity distributions, such as the isotropic and exponential ones. Also, the isotropic directivity lens is fabricated and the beam pattern is measured to verify the effectiveness. With a real Lambertian top emitting white light LED as the source, the experimental results agree well with the simulation ones, which provides high directivity isotropy (more than 80%). This scheme takes Fresnel loss of the lens into consideration and can also predict the efficiency of the lens; it may find applications in lighting or illumination engineering where directivity transformation are required.

Index Terms: Freeform lens, illumination, Lambertian source, directivity transformation, flux partition method.

1. Introduction

The need for high quality illumination has been increasing recently, particularly due to the emergence of new types of the light sources, such as LEDs. They are widely used in indoor/outdoor lighting, automobile headlights, etc., because they are more compact, long-life, energy-saving, compared with the traditional tungsten filament lamps [1]–[4]. Two important properties for illumination are the distributions of intensity, and illuminance at specific distance. It is known from basic radiometry that in far-field the two quantities can be transformed to each other, as explained in next section. Thus for specific far-field illumination distribution, the directivity (also called as beam pattern or intensity distribution, the terminologies used interchangeably) or the illuminance requirement are equally important and applicable. Usually the control of either intensity or illuminance distributions are achieved by the usage of second lenses or reflectors that are designed for those requirements [5]–[7]. The lens or reflector design can be characterized by various traits, such as standard form or free form [8], point-like source (zero éntendue) or extended source [9], [10], and with or without the rotational (cylindrical) symmetry [8]. Basically there are two approaches for the design task: the optimization way and the direct one. The former usually needs to parametrize the surface and choose suitable merit functions that can be approached by keeping adjusting the parameters with
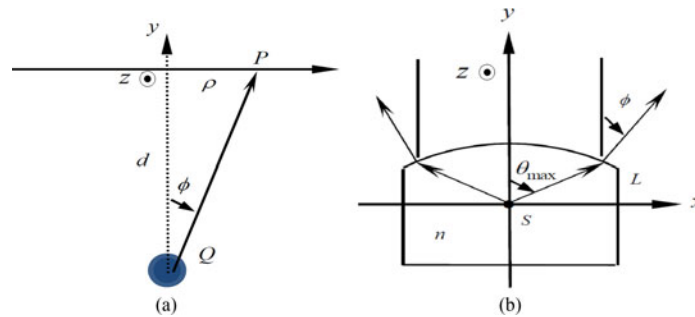
Fig. 1. (a) The schematic configuration and symbols for the illuminant Q with cylindrical symmetry. (b) The geometry, coordinate system, and the notations for an emitter S and a lens L.

trial-and-error or feedback design [11], [12]. This approach is usually time-consuming and is strongly sensitive to the starting point of the optimization. The direct approach obtains the lens profile directly and usually contains two strategies: mathematic or geometric ways. The former constructs mathematical equations (or partial differential equations) required to be satisfied with light source properties and prescribed illumination demands [13], [14]. There are some powerful methods such as simultaneous multiple surfaces (SMS), flow-lines [5], and Monge-Ampére equation [15]. The geometric way usually needs to discretize the illuminance or intensity distributions, and uses optical law, flux conservation, and/or basic conic surfaces to build the lens surfaces [16]–[19], such as supporting paraboloids [20], source-target [21], [22], generalized functional method [23], and flux partition method [24], [25]. The last method was proposed by the authors, which successfully provides highly uniform illumination and collimated beam for a Lambertian LED chip source, and it is the first one to take the Fresnel loss of the lens interface into considerations. Since highly transparent material such as PMMA, epoxy, or silicone are used in lens fabrication, Fresnel reflection is the main loss of the lens for a high efficiency design; it should be taken into consideration especially when the incident angle is large, which is not uncommon for practical lens shapes.

In this work, a refractive freeform lens design for arbitrary directivity shaping with cylindrical symmetry is proposed. It is a direct geometric method and easy to be implemented with high efficiency. This method modifies the previous optical flux partition one, and the comparisons and differences between them are given later. The principle and procedures are introduced first, followed by the simulations to check its effectiveness. One of its sample applications is fabricated and tested, which shapes the Lambertian pattern into an isotropic one. The measured results verify its validity and feasibility.

2. Methodology

As shown in Fig. 1(a), if a light lamp Q has the cylindrical symmetry intensity distribution $J(\phi)$, then for a point P that lies at a flat screen in far-field with vertical distance d from the source and horizontal distance ρ from the y axis, the illuminance $E(\rho)$ at P for is [26]

$$E(\rho) = J(\phi) \cdot \frac{\cos^3 \phi}{d^2} \tag{1}$$

Thus $E(\rho)$ and $J(\phi)$ are related and can be transformed into each other in far field, and we will focus on the shaping of the intensity distribution. Now consider the lamp Q is made of a package lens L and a light source S located at the origin of the x-y coordinates, as shown in Fig. 1(b). The source S emits light into upper space (positive y axis) and it has the cylindrical symmetry directivity form

$$I(\theta) = I_0 \cdot i(\theta) \tag{2}$$

TABLE 1

Symbols and Related Flux Terms for Different Types of Sources

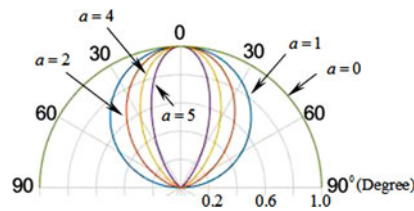| Source Type	Intensity Distribution	Optical Flux between angle 0 and θ:	Optical Flux between θ_1 and θ_2
General	$I(\theta) = I_0 \cdot i(\theta)$	$\Phi(0 : \theta) = 2\pi I_0 \int_0^\theta i(\theta') \sin(\theta')\, d\theta'$	$\Phi(\theta_1 : \theta_2) = \Phi(0 : \theta_2) - \Phi(0 : \theta_1)$
Exponential	$I_{\exp}(\theta) = I_0 \cdot \cos^a(\theta)$	$\Phi_{\exp}(0 : \theta) = \frac{2\pi I_0 [1 - \cos^{a+1}(\theta)]}{a+1}$	$\Phi_{\exp}(\theta_1 : \theta_2) = \Phi_{\exp}(0 : \theta_2) - \Phi_{\exp}(0 : \theta_1)$
$a = 0$ (isotropic)	$I_{\exp}(a = 0, \theta) = I_0$	$\Phi_{\exp}(a = 0, 0 : \theta) = 2\pi I_0 [1 - \cos(\theta)]$	$\Phi_{\exp}(a = 0, \theta_1 : \theta_2) = 2\pi I_0 [\cos(\theta_1) - \cos(\theta_2)]$
$a = 1$ Lambertian	$I_{\exp}(a = 1, \theta) = I_0 \cos(\theta)$	$\Phi_{\exp}(a = 1, 0 : \theta) = \pi I_0 \sin^2(\theta)$	$\Phi_{\exp}(a = 1, \theta_1 : \theta_2) = \pi I_0 [\sin^2(\theta_2) - \sin^2(\theta_1)]$

Fig. 2. The polar intensity distributions for an exponential intensity source with different values of exponents.

where I_0 is the maximum intensity and $i(\theta)$ is the normalized directivity. Thus we use the angle notations θ and Φ respectively to indicate angle variables for the original beam pattern ($i(\theta)$ or $I(\theta)$) for the source S and the transformed one ($j(\phi)$ or $J(\phi)$) for lamp Q; both θ and ϕ are referred to the positive y-axis. Apparently we want to design the lens L to transform $i(\theta)$ into another required normalized directivity $j(\phi)$ of the lamp Q. As in (2), the full representation $J(\phi)$ is related with $j(\phi)$ as

$$J(\phi) = J_0 \cdot j(\phi) \qquad (3)$$

where J_0 is the maximum intensity after the beam shaping, and it can be decided by the optical flux conservation, as will be shown later. Since our strategy is based on the flux partition method and conservation of optical flux, some related quantities that will be used later are introduced in Table 1. Two directivity types are included: the general type and the exponential one. The former is denoted as arbitrary directivity $I(\theta)$ without specific functional form; the latter has the directivity form of

$$I_{\exp}(\theta) = I_0 \cdot \cos^a(\theta), \quad a = 0, 1, 2, 3..... \qquad (4)$$

The subscript exp of I denotes the exponential factor in the power of the cosine term. It is well known that exponential intensity sources are often used to describe the beam pattern of a packaged LED lamp [27], and its distribution is depicted in Fig. 2. When $a = 0$, it is isotropic directivity. When $a = 1$, it is called a Lambertian source, which is a typical directivity of bare LED chip. When the value of a is larger, the directivity is stronger and the divergent angle (full width at half maximum intensity, FWHM) is narrower, which is usually achieved and controlled by the LED lens package. The third column shows the flux between angle 0 and θ for a cylindrical symmetry intensity with the symbol $\Phi(0 : \theta)$; the fourth column shows the flux between angle θ_1 and θ_2 for a cylindrical symmetry intensity with the symbol $\Phi(\theta_1 : \theta_2)$. The third and fourth rows show corresponding terms for $a = 0$ and $a = 1$ for exponential directivity. Besides its wide applications in describing packaged LED lamps, the advantage of using exponential intensity sources is that the quantities $\Phi_{\exp}(0 : \theta)$ and $\Phi_{\exp}(\theta_1 : \theta_2)$ can be presented analytically, benefiting the modeling and calculations. Otherwise those terms need to be calculated numerically for a general intensity distribution. The exponential
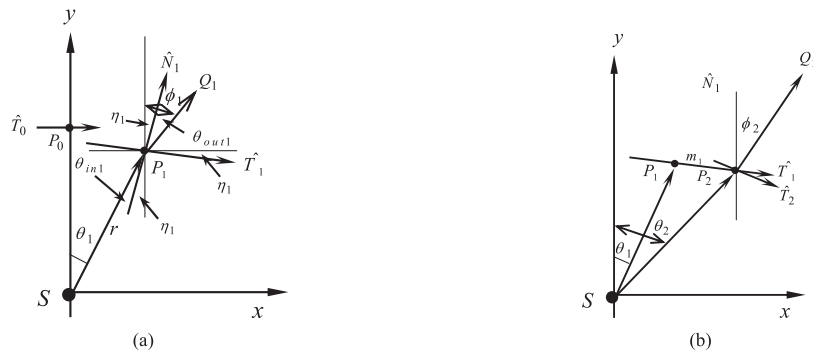
Fig. 3. Notations and geometry for lens design procedure. (a) Finding P1. (b) Finding P2.
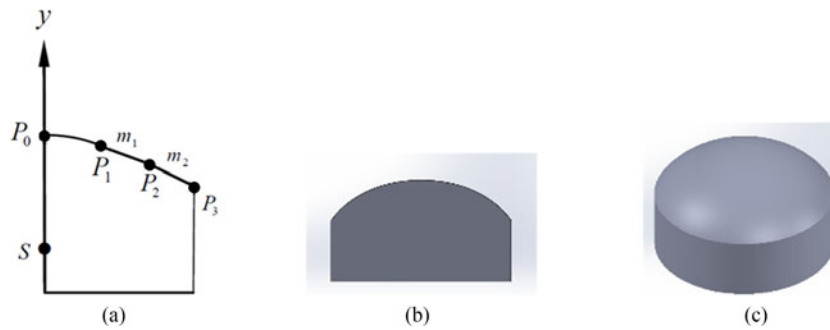

Fig. 4. (a) Illustration for the lens shape for N = 3. (b) Front view of the lens with N = 30. (c) Iso-angle view of (b).

intensity shaping lenses with our method will be used as the examples, say, changing from a Lambertian LED chip source ($a = 1$) to an isotropic LED lamp ($a = 0$) or to higher directivity with powers for $a = 2$, 3, 4, etc.

Table 1 can also be used to calculate the corresponding terms for shaped directivity $J(\phi) = J_0 \cdot j(\phi)$; note that the maximum intensity is J_0 and angle is ϕ when using it. For example, the flux between angle 0 and ϕ is $\Phi(0 : \phi) = 2\pi J_0 \int_0^\phi j(\phi') \sin(\phi') \, d\phi'$. Referring to Fig. 1, the purpose the lens L is to shape the general normalized directivity from $i(\theta)$ of the source S to $j(\phi)$ of the lamp Q, as in (2) and (3) respectively. The design procedures are illustrated as follows. (1) Find I_0 and $i(\theta)$ from data sheet or the intensity measurement of the source S. (2) Select the maximum angle θ_{max} within which the light is utilized, as denoted in Fig. 1(a). (3) Calculate the total optical flux over the range from 0 to θ_{max}, that is, $\Phi(0 : \theta_{max})$ in Table 1. (4) Select the maximum angle ϕ_{max} within which the lens or the lamp will deliver the flux and decide the required normalized directivity $j(\phi)$. The total flux over the range from 0 to θ_{max} is $\phi(0 : \phi_{max}) = 2\pi J_0 \int_0^{\phi_{max}} j(\phi') \sin(\phi') \, d\phi'$, with J_0 to be determined. (5) Assume the factor k is the efficiency coefficient that indicates the amount of $\Phi(0 : \theta_{max})$ transferred to $\Phi(0 : \phi_{max})$, i.e., $k \cdot \Phi(0 : \theta_{max}) = \Phi(0 : \phi_{max})$. The material absorption and Fresnel loss at the lens interface are the two factors affecting the transfer efficiency k; and the latter dominates k when highly transparent material with very low absorption is used for the lens with limited volume. Of course the value of k cannot be known in advance because it depends on the final shape of the lens. However, as we will show later, its value can be reasonably estimated first, which lies in between 0.7 to 0.95 for a decent lens shape. We will also discuss in next section what happens if the value of k is not properly estimated. Substituting $\Phi(0 : \theta_{max})$ and $\Phi(0 : \phi_{max})$ from above into the relation $k \cdot \Phi(0 : \theta_{max}) = \Phi(0 : \phi_{max})$, J_0 can be decided as

$$J_0 = k \cdot I_0 \int_0^{\theta_{max}} i(\theta') \sin(\theta') \, d\theta' \Big/ \int_0^{\phi_{max}} j(\phi') \sin(\phi') \, d\phi' \qquad (5)$$
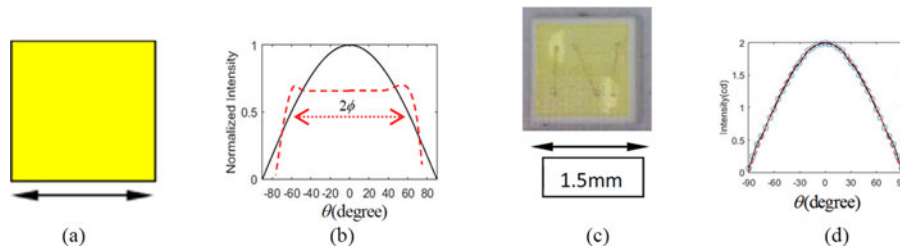
Fig. 5. (a) The square with side d is used to model a surface emitting light source S. (b) The linear intensity profile for two distributions. Solid black line is the Lambertian intensity of the source and the dashed red line is the isotropic distribution after shaping. (c) The picture of a real white light LED for a later experiment. (d) The measured beam pattern of the LED (blue circles), which well matches the Lambertian distribution (red line).

TABLE 2

Intensity Distribution, Horizontal Cut Value, and Isotropy for the Designed Lens With Different Partition Number

N	6	10	20	30
Intensity Distribution				
Horizon Cut Value				
Isotropy (%)	68	78	83	88

Once J_0 is found, $J(\phi)$ and the related flux quantiles, like those in Table 1, can be completely determined. (6) Select the number of partition N and divide θ_{max} equally into N partitions with each partition $\Delta\theta = \theta_{max}/N$. (7) Consider the first partition with angle $\theta_1 = \Delta\theta$, making a line with θ_1 from S as depicted in Fig. 3(a). Along this line, pick a point P_1 at distant r from S. $P_1(x_1, y_1)$ is the starting point of the lens profile and the value of r should consider the size of S, because the notion of directivity describes the beam pattern of an ideally point-like source. It is suggested that r is at least 10 times larger than the source size. The coordinates of P_1 can be calculated easily with $x_1 = r*\sin\theta_1$, $y_1 = r*\cos\theta_1$. (8) Find the slope $m_1 = -\tan\eta_1$ at P_1 as follows. As shown in Fig. 3(a), $\hat{T}_1$ and $\hat{N}_1$ are the tangent and normal unit vectors at P_1 respectively. The light ray SP_1 is refracted and directed to P_1Q_1 making an angle ϕ_1 to the vertical, which needs to be found first. We can calculate the transmitted flux through lens in the first partition angle $\theta_1 = \Delta\theta$ with $\Phi_{out1} = \Phi(0 : \theta_1) \cdot T_1$, where the subscript *out1* denotes the output flux in first partition and T_1 is the average transmittance for the air-lens interface. From Fresnel equations, $T_1 = 1-, R_1$, and R_1 is the

average reflectance, which depends on the incident angles between θ_{in1} and θ_{in0}, for incident rays SP_1 and SP_0, as depicted in Fig. 3(a). However, θ_{in1} is not decided yet because the tangent vector $\hat{T}_1$ (or the normal vector $\hat{N}_1$) needs to be found. Nevertheless, it is reasonable to ask the $\hat{T}_0$ to be horizontal ($m_0 = 0$) for the normal incident ray SP_0, leading to $\theta_{in0} = 0$ (i.e., the ray just follows the y-axis; the way to find P_0 will be explained later). When the partition number N increases, the value of θ_1 is small, so is θ_{in1}; it is justified to use the *left* boundary (normal incidence ray) to calculate R_1 and T_1, with $R_1 = [(n-1)/(n+1)]^2$. Since Φ_{out1} is found, the angle ϕ_1 can be obtained using the flux conservation; that is

$$\Phi_{out1} = \Phi(0 : \theta_1) \cdot T_1 = \Phi(0 : \phi_1) \tag{6}$$

where $\Phi(0 : \phi_1) = 2\pi J_0 \int_0^{\phi_1} j(\phi') \sin(\phi') \, d\phi'$. Referring to Fig. 3(b), two relations can be found with the geometry, they are $\theta_{in1} = \theta_1 - \eta_1$ and $\theta_{out1} = \phi_1 - \eta_1$. Substituting above two equations into the Snell's law, $n \times \sin(\theta_{in1}) = 1 \times \sin(\theta_{out1})$ the only unknown η_1 can be derived when θ_1 and are known. Finally the slope $m_1 = -\tan \eta_1$ at P_1 is found. (9) Find $P_2(x_2, y_2)$ as the following. From P_1 making a line with the slope m_1 that intersects the line with $\theta_2 = 2\Delta\theta$ from S as shown in Fig. 3(b). Since the equation of the two straight lines are known, the coordinates can be solved as

$$x_2 = \frac{m_1 x_1 - y_1}{m_1 - m_{S2}}, \quad y_2 = \frac{m_{S2}(m_1 x_1 - y_1)}{m_1 - m_{S2}} \tag{7}$$

where m_{S2} is the slope of SP_2. (10) Find m_2 at $P_2(x_2, y_2)$. Again, we calculate the transmitted flux in the second partition angle with $\Phi_{out2} = \Phi(\theta_1 : \theta_2) \cdot T_2(\theta_{in1}, \theta_{out1})$ from $\theta_1 = \Delta\theta$ to $\theta_2 = 2\Delta\theta$. Note that again the left boundary ray SP_1, with incident angle θ_{in1} and refraction angle θ_{out1}, already found in last step, is used to calculate the transmitted flux in second partition. The transmittance between the lens-air interface for oblique incident angle θ_{in} and refracted angle θ_{out}, by Fresnell equation [14], is $T(\theta_{in}, \theta_{out}) = 1 - R(\theta_{in}, \theta_{out})$ with

$$R(\theta_{in}, \theta_{out}) = \frac{1}{2} \left\{ \left[\frac{\sin^2(\theta_{in} - \theta_{out})}{\sin^2(\theta_{in} + \theta_{out})} \right] + \left[\frac{\tan^2(\theta_{in} - \theta_{out})}{\tan^2(\theta_{in} + \theta_{out})} \right] \right\} \tag{8}$$

Similar to the first partition, ϕ_2 can be obtained by requiring that the flux Φ_{out2} is equal to the flux in solid angle between ϕ_1 and ϕ_2, that is
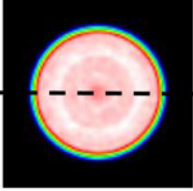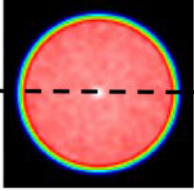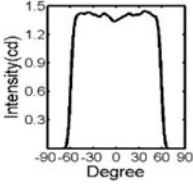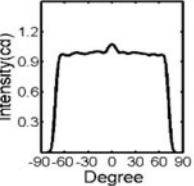
$$\Phi_{out2} = \Phi(\theta_1 : \theta_2) \cdot T_2(\theta_{in1}, \theta_{out1}) = \Phi(\phi_1 : \phi_2) \tag{9}$$

The same geometry in Fig. 3(a) can be used for the second partition to find η_2 by substituting $\theta_{in2} = \theta_2 - \eta_2$ and $\theta_{out2} = \phi_2 - \eta_2$ into the Snell's law, $n \times \sin(\theta_{in2}) = 1 \times \sin(\theta_{out2})$; and the slope is $m_2 = -\tan \eta_2$. (11) Repeat steps 9 and 10 to find all other points Pn and slopes m_n for $n = 3$ to N. (12) Find $P_0(x_0 = 0, y_0)$ and the profile between P_0 and P_1. Let us use a parabola $y = sx^2 + tx + c$ to describe the shape. There are 3 unknowns (s, t, c) and 3 conditions are needed to solve them, which should be m_1, $P_1(x_1, y_1)$, and $m_0 = 0$. The results are $t = 0$, $s = m_1/(2 \times 1)$, $c = y_0 = y_1 - (x_1 m_1/2)$. (13) Finally, we simply draw the parabola from P_0 and P_1 and then connect points P_1, P_2, ... to P_N with straight lines. From P_N we can draw a vertical line to some point below S and make a horizontal line that closes the lens shape, as indicated in Fig. 4(a) for N = 3. (14) Revolve this 2D shape with respect to y-axis to obtain the 3D shape with cylindrical symmetry. Fig. 4(b) and (c) show an example lens's front view and iso-angle view respectively, which is an intensity shaping lens that shapes an exponential intensity sources from $a = 1$ (Lambertian type) to $a = 0$ (isotropic type), with $\theta_{max} = \phi_{max} = 60°$, refraction index $n = 1.6$ (for Polycarbonate, used in experiment later), and N = 30.

3. Simulation Results

In order to verify the correctness of this method, the simulations are performed by a software called Optisworks first, and one of the simulated results is experimentally tested for its feasibility and effectiveness. For convenience of calculations, the exponential intensity sources are used as

TABLE 3
Intensity Distribution for k = 1.0 and 0.7 With N = 30.

k	1.0	0.7
Intensity Distribution		
Horizon Cut Value		
Isotropy (%)	87	86

the examples. The light source is modeled as a small surface-emitting square with length d, (see Fig. 5(a)) and has Lambertian intensity distribution, as the solid black line shown in Fig. 5(b). These properties of the light source are consistent with a real white light LED that is used in a later experiment; the picture of it is shown in Fig. 5(c) and its directivity is measured as in Fig. 5(d), which matches the Lambertian distribution well. Some parameters are set for simulations as the following, which are consistent with the experiment. As found in the Fig. 5(c), the size of the LED is about 1.5 mm *1.5 mm; thus the length d is set as 1.5 mm in Fig. 5(a) for the simulation. The central maximum intensity I_0 measured under 10 mA constant current driving condition is 2.0 cd with total flux about 6.2 lm; Thus this value of $I_0 = 2.0$ cd is used for the simulation. The material of the lens is PC (Polycarbonate), with the refraction index n = 1.6. Here the value of efficiency coefficient k is first guessed at 0.9. The distant r at step (7) is set as 20 mm, which is 10 times larger than the size of LED, as suggested. We set $\theta_{max} = 60°$, the source flux inside this solid angle is $\Phi_T = \pi I_0 \sin^2(\theta_{max}) \sim 4.6$ lm, containing 75% of the total LED flux.

The first example is to shape the intensity from the above LED Lambertian type $I_{exp}(a = 1, \theta) = I_0 \cos(\theta)$ into isotropic type $J_{exp}(a = 0, \phi) = J_0$ with $\phi_{max} = 60°$, which are depicted in Fig. 5(b) with black solid line and red dashed line respectively. The transformed isotropic beam pattern can provide uniform illuminance for curved spherical screen. As seen from Fig. 5(b), the intensity decreases from I_0 when the angle increases and it drops to about $I_0/2$ at $\theta = \pm60°$, and the directivity is not isotropic in this interval. Let us define a figure of merit, isotropy (the intensity distribution uniformity within an angle range from 0 to $\pm\theta$) as

$$\text{Isotropy} = (I_{min}/I_{max})^*100\% \tag{10}$$

where I_{max} and I_{min} are the maximum and minimum intensity in that angle range. Thus taking the distribution in Fig. 5(b) as the example, if the range is from 0 to $\pm60°$, its isotropy is 50%.

Table 2 shows the simulations results with this method for different partition number N (first row). The angular resolution for directivity is set with 2° and 10^7 light rays are used. In second and third row, the directivity and its horizon cut values (the dashed line in second row) are shown respectively. The forth row denotes the isotropy in the interested angle range ($-60°$ to $60°$, the horizontal arrows
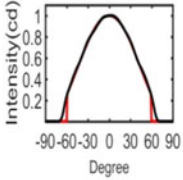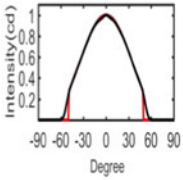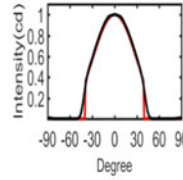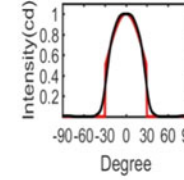
TABLE 4

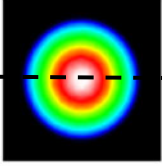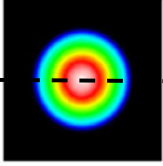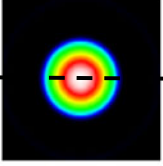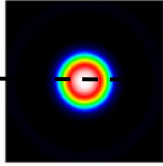Intensity Distribution, Horizontal Cut Value for the Case From a $= 1$ to b $= 4$ With Different Partition Number N

N	10	30	90	180
Intensity Distribution				
Horizon Cut Value				
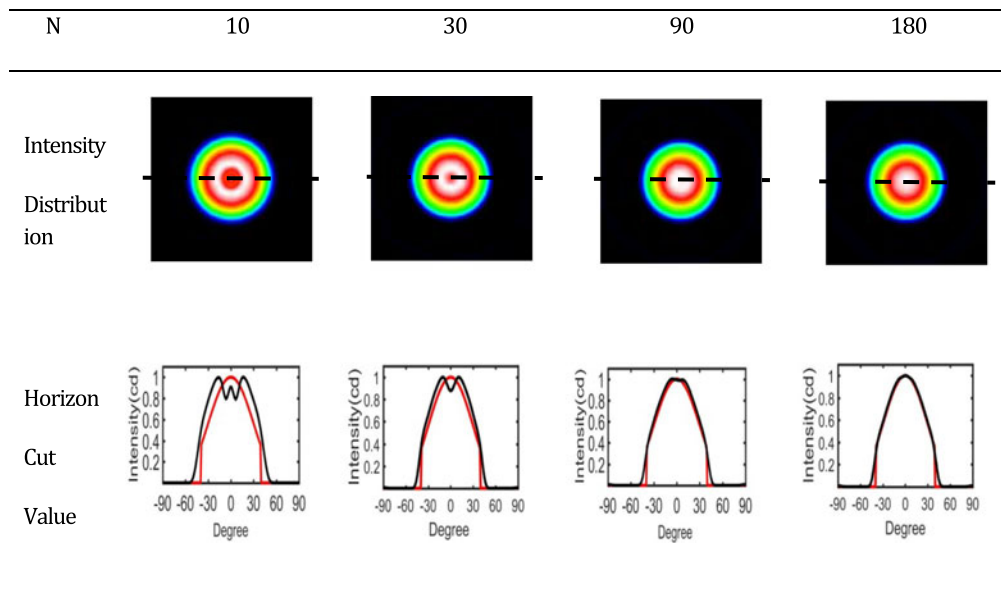
in the third row). Compared with the isotropy of 50% for the LED lamp, it increases to 68% and 78% for N = 6 and 10 respectively. When N = 20 or 30, isotropy goes to over 80%, which is good enough for most practical uses. Besides, the simulation shows that the average intensity is about 1.25 cd, which is close to the calculated $J_0 = 1.3$ cd with the relation $k \cdot \Phi(0 : \theta_{max}) = \Phi(0 : \phi_{max})$. The total simulated flux inside Ω_ϕ is 4.1 lm, which also agrees well with the calculated value $k\Phi_T$ with k = 0.9 and. $\Phi_T = 4.6$ lm. Now consider the situations when different values of k are estimat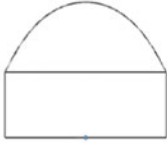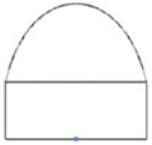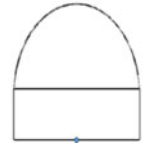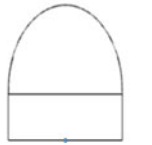ed. Table 3 shows the simulation results for $k = 1.0$ and $k = 0.7$ for N = 30. It is found that the most important feature – high isotropy – remains, the only differences lie in the angular extension and the average intensity; the FWHM of directivity is about 55°, 65°, and 75° for $k = 1.0, 0.9, 0.7$ respectively. The reason that smaller k has larger angular extension ϕ is because the value of J_0 is proportional to the estimated k value, as seem from (5); thus if k is underestimated, so is J_0. Consequently, the calculated angle ϕ in each partition is larger and the final ϕ_N is larger than the required angle ϕ_{max}. For example, using Table 1 and (3) for this case, we have $\phi_1 = \cos^{-1}[1 - (\Phi_{out1}/2\pi J_0)]$, which has bigger value of ϕ_1 when J_0 is smaller. Similar remarks applies to other values of ϕ_n. On the contrary, if k is overestimated, the final ϕ_N is smaller than the prescribed angle ϕ_{max}. This is a direct method, the final lens shape with proper partition numbers can be calculated in seconds or minutes with today's personal computers. Therefore, it should not be a big problem to get the k right with a few tries, and we only need to see if the final angular extension and required isotropy or directivity are achieved. Since we already know the effects of overestimating or underestimating k, judging to increase or decrease the present value of k is easy. It is worth noting that when the k is correctly found, not only the calculated ϕ_N matches designed ϕ_{max} but also the efficiency of the lens is obtained at this stage, which is a unique feature of this method.

The second example is to transform the $a = 1$ Lambertian intensity $i(\theta) = \cos(\theta)$ into the other exponential type with different power values of b in $j(\phi) = \cos^b(\phi)$. Table 4 shows the results with the proposed scheme with $k = 0.9$ to transform the directivity from $i(\theta) = \cos(\theta)$ to $\cos^4(\phi)$ with different partition number N. The red line is the required beam pattern $\cos^4(\phi)$ with $\phi_{max} = 40°$. It is found the resultant simulation beam patterns (black lines) agree well with the requested one when N is larger than 90. Comparing it with Table 2, it seems that the required N in this case to approach the required intensity distribution is larger than that of the case in Table 2, where N = 30 is good

TABLE 5

Intensity Distribution, Horizontal Cut Value, and for the Designed Lens From b = 2 to b = 5

Power b	2	3	4	5
ϕ_{max}	60°	50°	40°	30°
Intensity Distribution				
Horizon Cut Value				
Lens Shape				

enough. We also use the method to design the lens for other powers of *b* and ϕ_{max} under the condition of N = 180 and *k* = 0.9, as shown and indicated in Table 5. It shows that the simulations (black lines) meet the requirements (red lines) satisfactorily, which illustrates the effectivity of this method. The blue dot in the base line of each lens shape denotes the location of the light source.

The final example, with $i(\theta) = \cos(\theta)$, $j(\phi) = \sin^6(\phi)$, *k* = 0.82 and $\theta_{max} = \phi_{max} = 85°$, is given to illustrate the necessity of taking the Fresnel loss (FL) into consideration. As shown with the red lines in horizon-cut plot of Table 6, the requirement directivity is very different from the previous ones; this one has the biggest intensity at ϕ_{max} and the smallest value at the center. When FL is not taken consideration in the method, we simply set all the transmittance $T_n(\theta_{in}, \theta_{out}) = 1$ for n = 1 to N, such as those *T* in (6) and (9). As seen from Table 6, the simulation result (black line on the left) with FL matches the request directivity better than the one without FL (black line on the right). The iso-angle view 3D model of the correct lens is shown in Fig. 6(a), and its 2D section in Fig. 6(b). Note that 2D section for lens without FL is also plotted as indicated. Although the shape of the latter is not very different from the former, it already causes enough discrepancy in beam pattern, as seen from the Table. The transfer efficiency *k* is only 0.82 in this case, which is much lower than the previous two cases. It is because light rays must bend more drastically, compared to the previous two, to achieve the needed directivity, leading to larger incident angles and thus larger FL and lower *k*. Consequently under such a circumstance, failure to considering FL will cause the design result deviate more from the desired pattern, as we see here.

TABLE 6
Intensity Distribution, Horizontal Cut Value, and for Two Cases With/Without
Considering FC for $j(\phi) = \sin^6(\phi)$

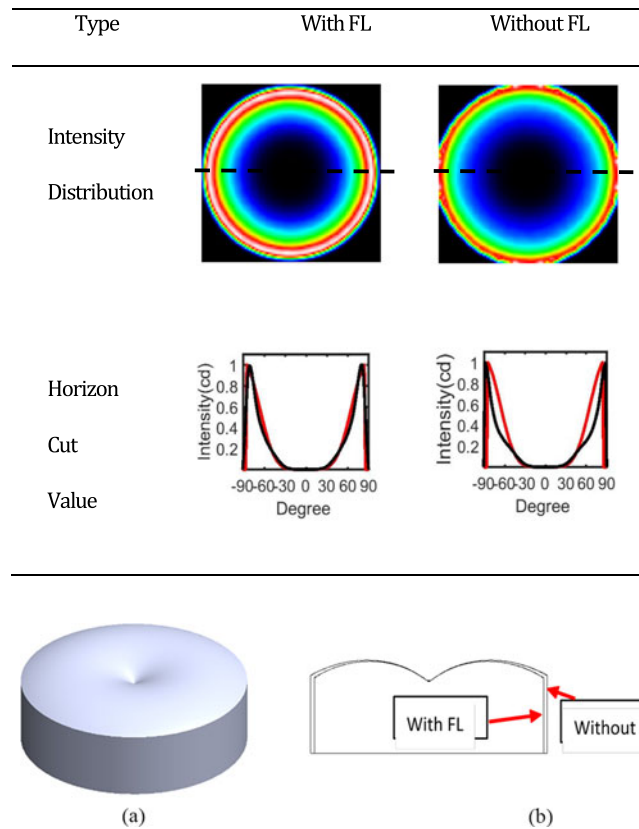| Type	With FL	Without FL
Intensity Distribution		
Horizon Cut Value		

Fig. 6. (a) The iso-angle view of 3D model for designed lens with FL. (b) The 2D section view of the lens with and without FL.
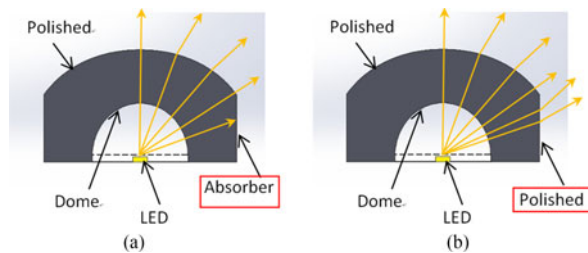

Fig. 7. (a) The final shape of the lens with a dome in the center and the vertical wall is an absorber. (b) The same lens with polished and transparent vertical wall.

It is worth comparing this modified method with the previous one, which is used to collimate a Lambertian LED source and to provide uniform illumination [20]. The main differences are the following: 1. The aim of this method is beam shaping, instead of the uniform illuminance and collimation. 2. The conservation of optical flux is used here, but achieving the target illuminance in each partition is utilized in [20]. 3. The slope m_n of P_n is easier to find in previous case cause the incident light rays are always refracted into vertical direction to maintain the collimation, but here the refracted rays are directed into different angle at each point P_n. 4. The final lens shape in previous case has some zigzags (see Fig. 4 in [20]), which maybe not easy to fabricate; but no such drawbacks exist in the present shape, as shown in Fig. 4(b) or Fig. 6(a), which has a much
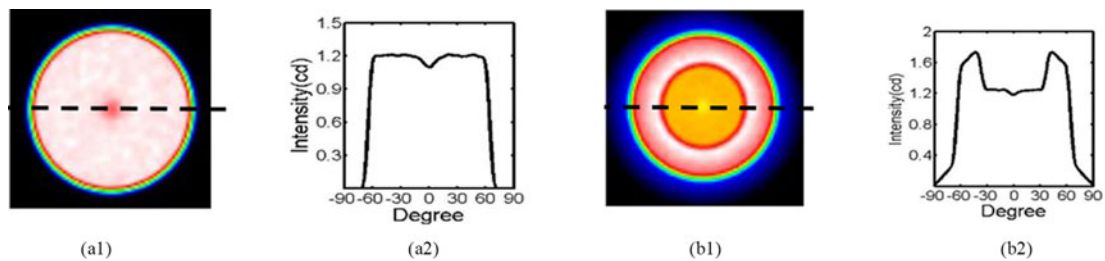
Fig. 8. (a1) and (a2) are the intensity distribution and horizon cut value for Fig. 7(a). (b1) and (b2) are the intensity distribution and horizon cut value for Fig. 7(b).
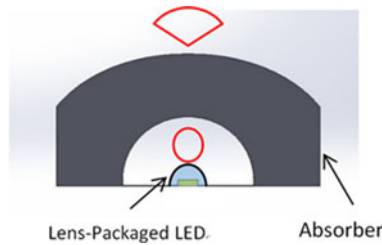

Fig. 9. The proposed domed second lens can be used as an isotropic beam pattern shaper for a package LED. The red shape on the top of the packaged LED and the lens represents the directivity of the package LED without and with the designed lens respectively.

more smooth shape when the partition number is big enough and facilitates the lens fabrication, as shown next.

4. Experimental Results

The first lens design example that shapes Lamberian pattern into isotropic beam is fabricated to verify its function. In the original design the LED source is immersed in the lens, which needs a molding process and is more suitable for mass production. However this process costs a lot and is time-consuming, which doesn't fit for the verification purpose. This difficulty can be overcome by digging a hollow semi-spherical dome in the lens, with the top emitting surface of package LED placed at the dome center, as shown in Fig. 7(a). The diameter of the dome is set as 10 mm; thus the light rays lie more or less in the center of the dome and they can penetrate the dome surface and, following the normal radial direction, go almost straight to the lens top surface, like the orange light rays in the figure. Since the dome introduces one more interface and thus induces more Fresnell loss (about 4% for normal incidence from the center), the value of k needs to be lowered and it is set at $k = 0.85$. With the same procedures, the final shape is shown in Fig. 7(a), including the dome. To double check the function of the lens with this modification, a simulation is performed and the result is shown is Fig. 8(a). It is found the isotropy (about 86%) and the angular extension still meet the requirement, compared with the original one (without the dome) in Table 2 ($N = 30$), except that the intensity in Fig. 8(a) drops a little bit, which is reasonable because the value of k is now 0.85, instead of 0.9. Another advantage of this domed configuration is that for some other lens-packaged LED with specific directivity, this hollow domed outer lens can correct its directivity (directivity shaping) and give required intensity distribution, as shown in Fig. 9; of course the size of the packaged LED should be considered when designing the space of the dome. Note that simulation results shown in Table 2 and Fig. 8(a) are obtained by setting the vertical wall of the lens as a perfect absorber, indicated by the red box in Fig. 7(a); thus the emitting the light rays can be only refracted by the top surface, as denoted in Fig. 7(a). However, if the wall is polished and transparent, rays beyond θ_{max} will be refracted by the wall, as shown in Fig. 7(b) and it has some effects on the isotropy of the original design, as the shown in Fig. 8(b). Most of the rays refracted

Fig. 10. (a1) and (a2) are respectively the front view and iso-angle view of the manufactured lens. (b1) and (b2) are the corresponding views of the same lens with a black tape applied to the vertical wall of the lens.
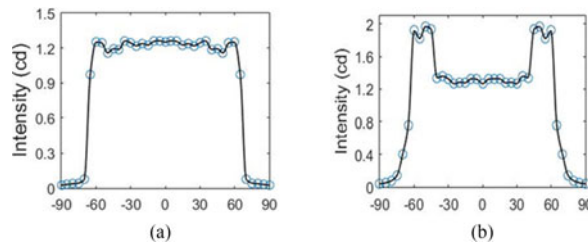

Fig. 11. (a) The measured directivity of the configuration in Fig. 10(a). (b) The measured directivity of the configuration in Fig. 10(b). The blue circles denote the measured data.

by the vertical wall contribute to the directivity from 45° to 60°. These factors should be taken into considerations when practically using the lens, as explained below.

The lens is manufactured by a much cheaper CNC (Computer Numerical Control) lathe technique, compared with the molding process, and the whole surface is polished, including the vertical wall and the dome, as shown in Fig. 10(a). As explained above, the light coming from the vertical wall affect the required isotropy. Thus a black tape is applied to the vertical wall to avoid these effects, as shown in Fig. 10(b), which absorbs most of the light refracted by the side wall. The intensity distribution of the taped second lens (see Fig. 10(b)) with LED (see Fig. 5(c)) is first measured with a goniometer (ISUZA Optics, model IGM-500) with 0.1° precision and the light detector (Minolta T-10 mA). The distance between the lamp and the detector is 30 cm. The result is shown in Fig. 11(a). The measured data are represented with blue circles and they are interpolated by a cubic curve. This configuration corresponds to simulated Fig. 7(a) and the experiment data agree well with the simulation one in Fig. 8(a2). When the tape is removed from the lens as in Fig. 10(a), corresponding to simulated Fig. 7(b), another measurement is taken, as shown in Fig. 11(b), which is also consistent with the simulation in Fig. 8(b2). The experimental results prove the correctness and feasibility of this design method.

5. Discussion and Conclusion

A new strategy to design free form lens that performs beam pattern transformation is presented in this work. The principle and procedures are introduced first and then with a Lambertian, different directivities transformation source are achieved to illustrate its validity. Nevertheless, in principle it can be applied to almost arbitrary beam shaping for any sources intensity distribution. Although it is powerful and easy to use, there are still some limitations. First, the intensity distribution must be cylindrical symmetric. However, we think it is possible to generalize it to situations without this symmetry if two dimensions general coordinates are used and the flux is partitioned in a different way. This target will be studied in the future. Second, not any desired directivity can be achieved; for example, if at some incident angle the calculated refracted angle is too big to meet the Snell's law, this scheme cannot work properly. With modified optical flux partition technique, this method is based on geometric optics, flux conservation, and Fresnel equations. The main features of this kind of flux partition method are that Fresnel loss is taken into consideration, which play an important

role for drastic directivity transform, and that the efficiency of the lens can be correctly found at the design stage. It also has the advantages of directness and speed, without using the iterative Monte Carlo ray-tracing simulation schemes or more complicate partial differential equations. The designed lens offering isotropic distribution is fabricated and tested, and the experimental results justify its effectiveness and feasibility. This method is expected to find wide applications in general beam shaping, particularly in illumination or related lighting fields.

References

[1] R. J. Koshel, *Illumination Engineering*, New York, NY, USA: Wiley, 2013, ch. 4.
[2] Y. Ding, X. Liu, Z.-R. Zheng, and P. F. Gu, "Freeform LED lens for uniform illumination," *Opt. Exp.*, vol. 16, no. 17, pp. 12958–12966, Aug. 2008.
[3] C. C. Sun, X.-H. Lee, I. Moreno, C.-H. Lee, Y.-W. Yu, T.-H. Yang, T.-Y. Chung, "Design of LED street lighting adapted for free-form roads," *IEEE Photon. J.*, vol. 9, no. 1, Feb 2017, Art. no. 8200213.
[4] Z. M. Zhu, H. Liu, and S.-M. Chen, "The design of diffuse reflective free-form surface for indirect illumination with high efficiency and uniformity," *IEEE Photon. J.*, vol. 7, no. 3, Jun. 2015, Art. no. 1600510.
[5] R. Winston, *Nonimaging Optics*. Amsterdam, The Netherlands: Elsevier, 2005.
[6] J. Rubinstein and G. Wolansky, "Intensity control with a free-form lens," *J. Opt. Soc. Amer. A*, vol. 24, no. 2, pp. 463–469, Feb. 2007.
[7] C.-Y. Tsai, "Free-form surface design method for a collimator TIR lens," *J. Opt. Soc. Amer. A*, vol. 33, no. 4, pp. 785–792, Apr. 2016.
[8] J. Chaves, *Introduction to Nonimaging Optics*. Boca Raton, FL, USA: CRC Press, 2008, ch. 8.
[9] R. Wu, C. Y. Huang, X. Zhu, H.-N. Cheng, and R. Liang, "Direct three-dimensional design of compact and ultra-efficient freeform lenses for extended light sources," *Optica*, vol. 3, no. 8, pp. 840–843, Aug. 2016.
[10] S. Hu, K. Du, T. Mei, L. Wan, and N. Zhu, "Ultra-compact LED lens with double freeform surfaces for uniform illumination," *Opt. Exp.*, vol. 23, no. 16, pp. 20350–20355, Aug. 2015.
[11] J. C. Bortz, N. E. Shatz, and D. Pitou, "Optimal design of a nonimaging projection lens for use with an LED source and a rectangular target," *Proc. SPIE 4092, Novel Opt. Syst. Design Optim. III*, vol. 4092, pp. 130–138, Oct. 2000, doi: 10.1117/12.402419.
[12] Y. Luo, Z. Feng, Y. Han, and H. Li, "Design of compact and smooth free-form optical system with uniform illuminance for LED source," *Opt. Exp.*, vol. 18, no. 9, pp. 9055–9063, Apr. 2010.
[13] F. Fournier and J. Rolland, "Optimization of freeform lightpipes for light-emitting-diode projectors," *Appl. Opt.*, vol. 47, no. 7, pp. 957–966, Mar. 2008.
[14] D. Ma, Z. Feng, and R. Liang, "Tailoring freeform illumination optics in a doublepole coordinate system," *Appl. Opt.*, vol. 54, no. 9, pp. 2395–2399, Mar. 2015.
[15] R. Wu *et al.*, "Freeform illumination design: A nonlinear boundary problem for the elliptic Monge–Ampére equation," *Opt. Lett.*, vol. 38, no. 2, pp. 229–231, Jan. 2013.
[16] J.-J. Chen, T.-Y. Wang, K.-L. Huang, T.-S. Liu, M.-D. Tsai, and C.-T. Lin, "Freeform lens design for LED collimating illumination," *Opt. Exp.*, vol. 20, no. 10, pp. 10984–10995, May 2012.
[17] J.-J. Chen and C.-T. Lin, "Freeform surface design for a light-emitting-diode based collimating lens," *Opt. Eng.*, vol. 49, no. 9, Sep. 2010, Art. no. 093001.
[18] W. Song, D. Cheng, Y. Liu, and Y. Wang, "Free-form illumination of a refractive surface using multiple-faceted refractors," *Appl. Opt.*, vol. 54, no. 28, pp. E1–E7, Oct. 2015.
[19] C.-M. Tsai, "Uniformity and collimation of incoherence Gaussian beam with divergence based on only one Fresnel surface," *IEEE Photon. J.*, vol. 8, no. 6, Dec 2016, Art. no. 6500509.
[20] V. Oliker, "Mathematical aspects of design of beam shaping surfaces in geometrical optics," in *Trends in Nonlinear Analysis*. New York, NY, USA: Springer, 2002, pp. 191–222.
[21] F. R. Fournier, W. J. Cassarly, and J. P. Rolland, "Fast freeform reflector generation using source-target maps," *Opt. Exp.*, vol. 18, no. 5, pp. 5295–5304, Mar. 2010.
[22] J.-J. Chen, Z.-Y. Huang, T.-S. Liu, M.-D. Tsai, and K.-L. Huang, "Freeform lens design for light-emitting diode uniform illumination by using a method of source–target luminous intensity mapping," *Appl. Opt.*, vol. 54, no. 28, pp. E146–E152, Oct. 2015.
[23] J. Bortz and N. Shatz, "Generalized functional method of nonimaging optical design," *Proc. SPIE 6338, Nonimag. Opt. Efficient Illumination Syst. III*, vol. 6338, Aug. 2006, Art. no. 633805, doi: 10.1117/12.678600.
[24] H.-C. Hsu and P. Han, "Optical flux partition method for high uniformity illumination of a refractive lens," *Appl. Opt.*, vol. 53, no. 29, pp. H14–H19, Oct. 2014.
[25] H.-C. Hsu and P. Han, "High uniformity and directivity of a reflective device with optical flux partition method," *J. Display Technol.*, vol. 11, no. 12, pp. 1018–1022, Dec. 2015.
[26] W. R. McCluney, *Introduction to Radiometry and Photometry*, Norwood, MA, USA: Artech House, 1994.
[27] E. Uiga, *Optoelectronics*. Englewood Cliffs, NJ, USA, Prentice-Hall, 1995, pp. 32–33.